Practical Application of Direct Electron Detectors to EBSD Mapping in 2D and 3D

K.P.Mingard[a,*], M.Stewart[a], M.G.Gee[a], S.Vespucci[b] and, C.Trager-Cowan[b]

[a]: National Physical Laboratory, Hampton Road, Teddington, Middlesex, TW11 0LW, United Kingdom

[b]: Department of Physics, SUPA, University of Strathclyde, Glasgow G4 0NG,United Kingdom
* corresponding author: ken.mingard@npl.co.uk

Abstract

The use of a direct electron detector for the simple acquisition of 2D electron backscatter diffraction (EBSD) maps and 3D EBSD datasets with a static sample geometry has been demonstrated in a focused ion beam scanning electron microscope. The small size and flexible connection of the Medipix direct electron detector enabled the mounting of sample and detector on the same stage at the short working distance required for the FIB. Comparison of 3D EBSD datasets acquired by this means and with conventional phosphor based EBSD detectors requiring sample movement showed that the former method with a static sample gave improved slice registration. However, for this sample detector configuration, significant heating by the detector caused sample drift. This drift and ion beam reheating both necessitated the use of fiducial marks to maintain stability during data acquisition.

Highlights

- A direct electron detector has been used to acquire electron backscatter diffraction patterns to produce EBSD maps
- The small detector size allows the simple implementation of a static geometry for 3D EBSD mapping in a focused ion beam scanning electron microscope
- The static geometry reduces random misalignments of sequential EBSD maps compared with that produced by the standard moving sample set up
- Significant heating effects by the detector need to be allowed for to realise this reduced variation in position

Keywords

EBSD, Direct electron detector, Medipix, 3D EBSD, SEM image drift, Focused Ion Beam

Practical Application of Direct Electron Detectors to EBSD Mapping in 2D and 3D

K.P.Mingard[a], M.Stewart[a], M.G.Gee[a], S.Vespucci[b] and, C.Trager-Cowan[b]

[a]: National Physical Laboratory, Hampton Road, Teddington, Middlesex, TW11 0LW, United Kingdom

[b]: Department of Physics, SUPA, University of Strathclyde, Glasgow G4 0NG,United Kingdom

1. Introduction

The use of CMOS sensors to directly detect diffracted electrons in the SEM and thus acquire EBSPs has been demonstrated to produce very high quality patterns [1,2]. These patterns yield enhanced information from the diffraction band structure in comparison with the conventional indirect EBSD cameras which use a phosphor to detect the electrons followed by a lens and a CCD to capture the light produced by the phosphor [3]. The first approach for direct electron EBSP acquisition [1] used a back-thinned active pixel sensor with approximately 1000x1000 pixels and showed that, with optimum back-thinning by reactive ion etching, pattern acquisition times of between 0.2 and 20 s were required with 20 keV incident beams. Vespucci et al [2] used a hybrid pixel Medipix sensor [4,5] and demonstrated that with this 256x256 pixel digital detection chip, in which the acquisition parameters of each pixel can be adjusted separately, energy thresholding is possible. Thresholding gave a further improvement in the pattern quality achievable by reduction in counts of background, low energy, electrons. Typical acquisition times of between 1 and 50 s were shown to give extremely high quality patterns and discernible EBSD patterns could still be acquired in times as low as 0.5 ms. Times below ≈10 ms would be needed for conventional EBSD mapping of large areas.

The current work has investigated the practical application of the medipix detector to mapping of samples by acquisition of multiple EBSPs with short acquisition times and at the same time exploiting a significant advantage of the detector, its small size, to produce a simple system for 3D EBSD in a FIB-SEM without the need to move the sample between FIB milling and EBSD acquisition positions..

A static system such as this, which avoids the usual requirement for 3D EBSD of moving the sample backwards and forwards from the FIB milling position to the correct orientation for EBSD, has already been demonstrated by Guyon et al [6], building on the principle shown in, for example, [7]. They clearly showed that a conventional phosphor screen EBSD detector mounted at 15.3° from the normal to the plane containing the FIB enables this static 3D EBSD geometry, with a strong potential for improved accuracy in the alignment of data from successive slices as well as improved reliability in the process of data acquisition itself. This geometry does however present challenges for the fitting of the EBSD detector to the majority of FIB-SEMs, from the point of view of a) fitting an appropriately positioned port to allow insertion of the conventional EBSD detector and b) enabling the EBSD detector to work at the short working distances (typically 4-5 mm) required by most FIB-SEMs. The direct electron detector enables both these difficulties to be overcome in a simple manner but introduces challenges of its own which are discussed in this paper by comparing preliminary results from 3D EBSD datasets acquired on the same microscope with either the static sample and direct electron detector or a conventional moving sample and phosphor detector.

2. Experimental Details

All the work described was carried out in a Zeiss Auriga 60 FIB-SEM. Conventional 3D EBSD analysis [7,8] with a phosphor based detector was carried out using an Oxford Instruments (OI) Nordlys F EBSD detector inserted into the chamber directly beneath the FIB column and perpendicular to the sample tilt axis. This geometry requires sample movement to alternate between milling and EBSD acquisition of: a 180° rotation, a change in sample height (Z) from 5 to 14 mm working distance, followed by small adjustments in X and Y stage positions. Stage coordinates for these parameters were stored for the two positions and used by the OI Fast Acquisition software, which also controlled the EBSD acquisition and the calling of Zeiss milling routines. An image correlation routine, applied to a fiducial mark adjacent to the area of interest, was used after each movement to shift the ion or electron beam to maintain alignment between successive FIB milling slices or EBSD maps. Figures 1a-b shows example images of the sample and fiducial marks in the FIB and EBSD positions. The principal directions (x_S, y_S for the SEM image and x_F, y_F for the FIB image) used for beam shifts are indicated for each position in relation to the principal directions used in the final 3D dataset.

3D EBSD datasets were acquired using two different sample holders shown in Figure 1d. The first was a large holder which required a translation of 50 mm parallel to the tilt (X-) axis (parallel to both x_S and x_F axes) before it could be rotated without hitting the EBSD detector, and a reverse translation after the rotation followed by small correctional shifts in the Y axis perpendicular to the tilt axis; in the following text this method is described as the Move and Rotate mode. The second was a much smaller holder which could be safely rotated in front of the EBSD detector with only small X and Y movements to compensate for unavoidable small displacements of the site of interest from the rotational axis (subsequently described as the Rotate only mode). Both methods required the same z-stage movement between FIB and EBSD working distances. For capture of the electron backscatter diffraction patterns (EBSPs) the detector was run with 4x4 pixel binning, an acquisition time of 16 ms and a sample-detector distance of 18 mm to allow for sample movement towards the detector during rotation between FIB and EBSD position. A typical EBSP is shown in Figure 2a: the pattern centre for this case was 0.48, 0.66, 0.64 for x*,y*,z* and an indexing success rate of ≈70% was achieved. The mapped area was approximately 30 x 30 µm with a 0.2 µm step size, requiring a time of 6 min 30 s to map, 2 min 52 s to mill plus an average of about 5 min per cycle for the rotation and image correlation steps between EBSD and FIB positions, and about 6 min per cycle for these steps when the 50 mm movement as well as rotation was required (i.e. a total of approximately 14 min for rotate only and 15 min for move and rotate).

For the direct electron detection EBSD acquisition (the static mode, as no sample movement was needed during acquisition), the angular positioning of the sample to the FIB and SEM columns described by Guyon [6] was used. For typical FIB-SEM setups there are two possible positions for static EBSD, oriented symmetrically about the FIB-SEM plane. Here we have used the forward facing position as it enables the detector/sample to slide in and out fixed to the front door, whereas Guyon [6] used the rear position. The sample was mounted on a pin stub which was then clamped to a *4* axis system (x,y,z and tilt) of Smaract piezo electric actuators; these actuators were themselves mounted on a baseplate which could be attached to the standard microscope stage. This stage was centred and rotated to the correct angle prior to mounting the baseplate after which it did not require movement during subsequent experiments

The direct electron detector was then attached to the same baseplate as the sample/Smaract actuators and thus the whole system could be simply inserted as a single assembly into the

microscope with the detector oriented at the required 15.3° to the normal to the SEM/FIB plane. The sample-detector distance was thus fixed at ≈ 5 mm, but the position to be analysed on the sample edge could be selected by movement of the Smaract stages. Figure 3 shows a schematic representation of the arrangement of sample and detector.

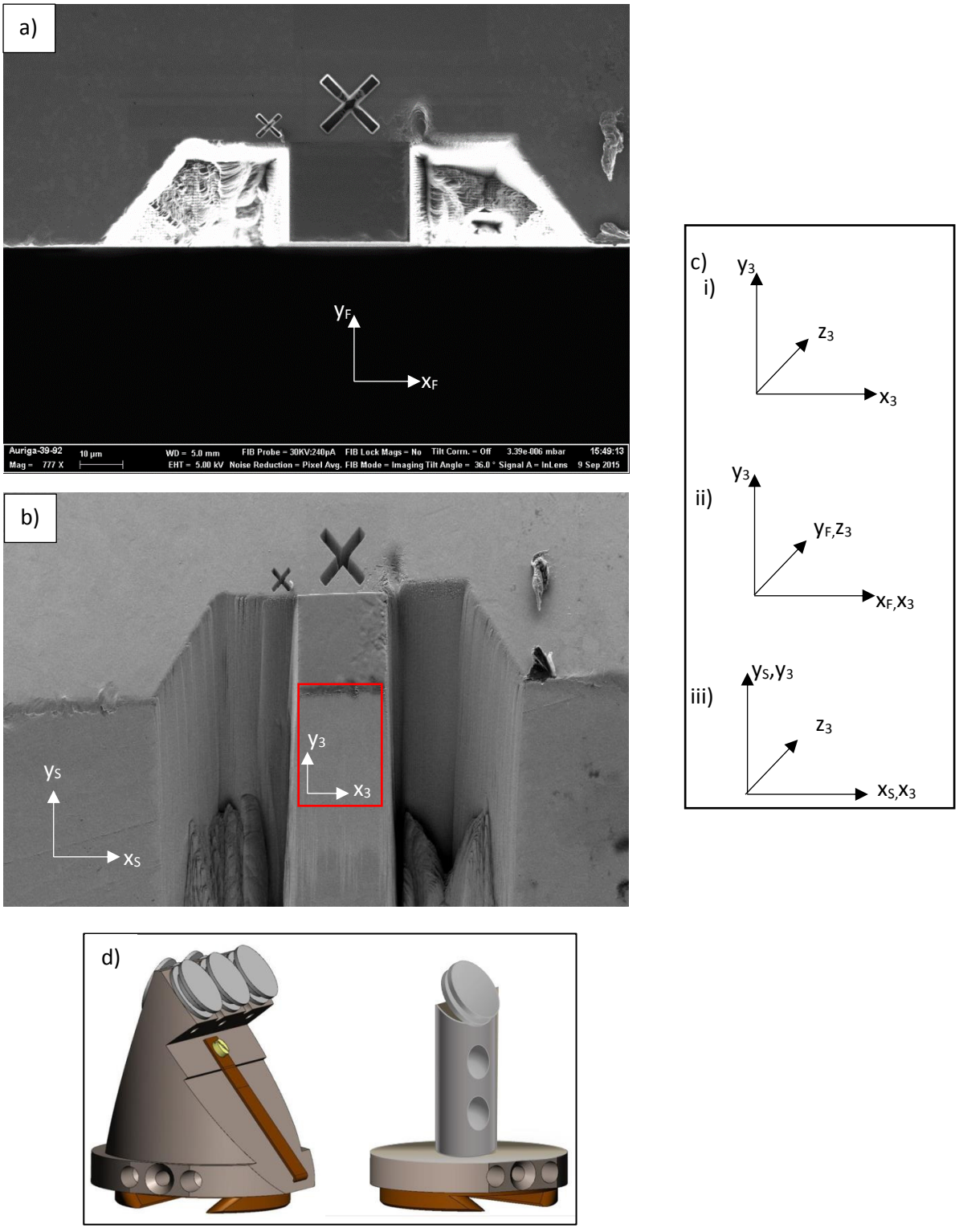

Figure 1. Images of milled region and fiducial marks used for alignment for the conventional 3D EBSD acquisition. a) FIB image, b) SEM image with box indicating area mapped by EBSD, c) schematic to show relationship between the axes of the FIB and SEM beam movements and the final 3D

reconstruction: i)3D reconstruction axes, ii) FIB x_F, y_F axes in relation to 3D axes and iii) SEM x_S, y_S axes in relation to 3D axes. D) Sample holders used for Move and rotate mode (left) and Rotate only mode (right)

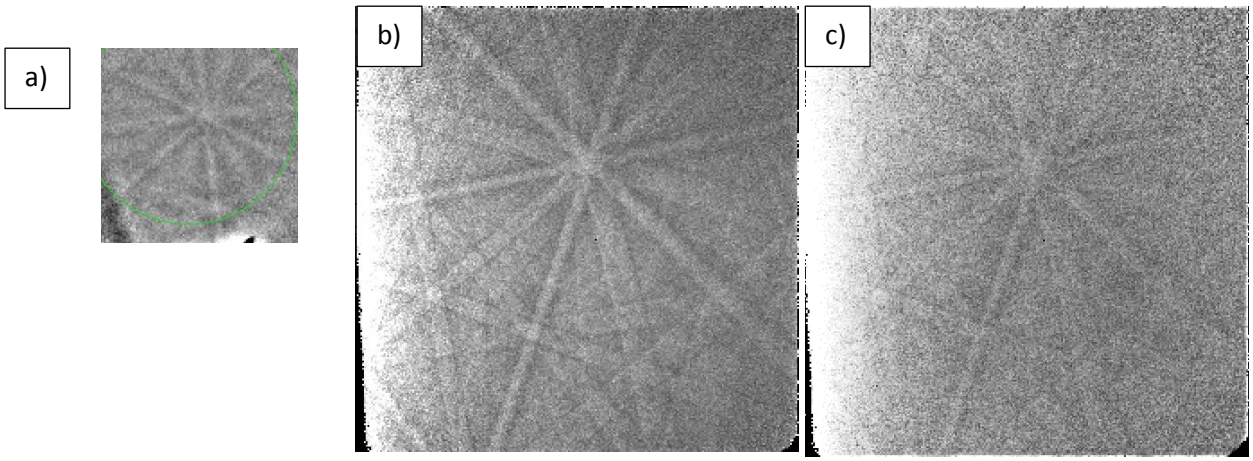

Figure 2. Example EBSPs, scaled by size in pixels, acquired with a) Conventional detector, 16ms acquisition time with 4x4 binning (cut down to 110 x110 pixels to omit shadows caused by sample edges, with green circle showing area of pattern used for indexing), and b) Direct detector (25 ms) and c) Direct detector (5 ms): both the latter are 256x256 pixels. All patterns acquired at 30 kV with a 10 nA current

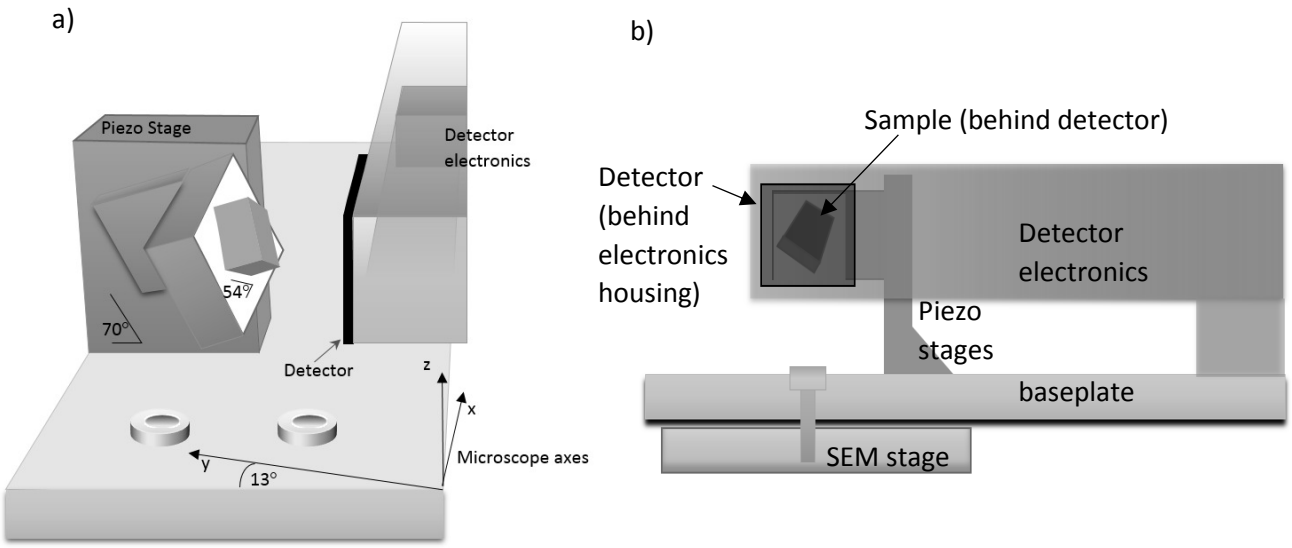

Figure 3. Schematic drawings (not to scale) of the arrangement of direct detector and sample on a common baseplate for single mounting onto SEM stage. a) perspective view, b) plan view seen from rear of detector

The direct electron detector was a Medipix2 “Modupix” detector produced by Advacam [9], with the same operating principles as that used by Vespucci et al [2] but with a thin Al coating over the whole surface of the detector. This coating is likely to prevent low energy electrons (< 5keV) reaching the

detector but probably has no significant effect on the intensity of the EBSPs acquired at 30keV, although no direct comparison has been carried out. As described in the following paragraphs, any effect of the coating on EBSP acquisition time was clearly negligible compared with other constraints.

The entire milling and EBSD mapping process was controlled by in-house software written with the Zeiss API software suite, but image correlation of a fiducial mark using the same routine described previously was also employed at each change between FIB milling and SEM EBSD acquisition. Initially this correlation was intended to simply monitor the stability of the system since it is commonly not used for static "slice and view" imaging without EBSD; however, as will be shown later, it was found to be necessary for adjustments to maintain image position. Figure 4 shows the orientation of the FIB and SEM images captured by the system and the principal directions used for beam shifts for each position in relation to the principal directions used in the final 3D dataset. The FIB image has a scan rotation added so the edge of the sample is parallel to the image x direction x_F. The SEM scan rotation was adjusted so that the direction of the 70° tilt is parallel to the SEM image y direction y_S so that the tilt correction is correctly implemented. This means that in contrast to the other modes the edge of the sample is not parallel to x_S and a rotation of around 54° is needed on the EBSD scan pattern to make it orthogonal to the sample edge. EBSD patterns acquired for each map were stored and subsequently indexed off-line using OI Flamenco or TSL OIM software.

For the direct detector, the EBSP acquisition time used was 25 ms; an example pattern is shown in Figure 2b. This acquisition time was 50% greater than that used with the conventional detector, but an indexing success rate of >95% was obtained and subsequent work has shown this time can be cut to at least 5 ms and still produce indexable patterns, as shown in Figure 2c. Both patterns are 256x256 pixels with a pattern centre of 0.49, 0.82, 0.39 for x*,y*,z*. With the detector size of only 14 mm, the z* value shows they were acquired with the detector much closer to the sample than for the conventional case. This proximity is possible because the size of the detector and because of the common mounting of the stage and detector. The improved pattern quality helped with the indexing success rate, but off-line indexing also enables indexing (Hough) settings to be used which might normally be avoided to maintain indexing speed.

However, the pattern acquisition rate was actually limited by the read-out speed of the Modupix read-out system controlling the Medipix 2 detector which added 30 ms to the time required for capture of each pattern and resulted in a total time of 9 min to map a 33 x 33 µm area with a step size of 0.33 µm. It is possible with different read-out electronics to achieve rates of at least 1400 Hz with Medipix 2 detectors [10] so it should be possible to achieve much faster EBSP acquisition than achieved here with improved electronics.

The following results compare three 3D EBSD datasets. The first two acquired with a fine grained recrystallized Ni superalloy used the conventional phosphor EBSD detector and geometry, firstly with the larger sample holder in the move and rotate mode and secondly with the small holder for the rotate only mode. The third dataset was acquired in the static mode with the direct electron detector, examining a partially recrystallized Ni superalloy.

In all three cases the samples were milled with a 30kV/2nA Ga ion beam. The beam was nudged by 200 nm from its previous position before milling each slice, and after each slice had been milled the surface exposed was mapped by EBSD with a 30 kV and ≈ 10 nA beam with the EBSD acquisition conditions described previously.

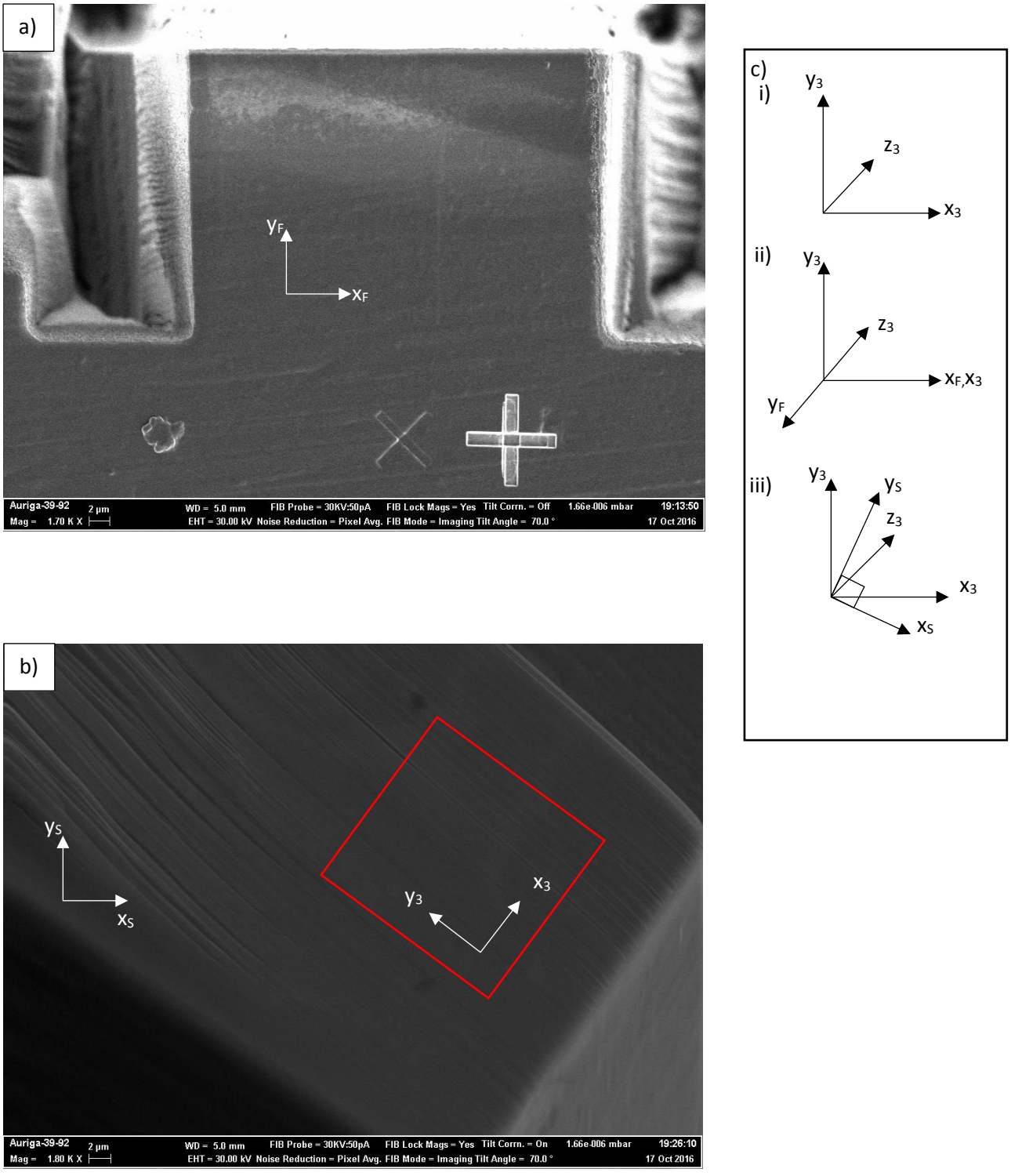

Figure 4. Images of milled region and fiducial marks used for alignment for the Direct Detector Static acquisition. a) FIB image, b) SEM image with box indicating area mapped by EBSD, c) schematic to show relationship between the axes of the FIB and SEM beam movements and the final 3D reconstruction: i) 3D reconstruction axes, ii) FIB x_F, y_F axes in relation to 3D axes and iii) SEM x_S, y_S axes in relation to 3D axes.

3. Results

3.1 Sample stability

The errors resulting from alternating between EBSD acquisition and milling were assessed using the correctional beam shifts determined from image correlation of the fiducial mark after each switch with the original ion beam image of the mark. Figure 5 shows the data for these beam shifts after excluding the additional 200 nm nudge required for each step to mill the next slice. Figure 5a shows the size of the correctional shift determined after each movement to the milling position, while Figure 5b shows the cumulative effect of these shifts relative to the original beam/sample position. The first set of data on the left of each graph shows the shifts x_F and y_F required for the Ni sample in the move and rotate mode/ conventional EBSD set up. The second set shows the shifts for the rotate only mode/conventional detector and third set for the static/direct electron detector mode.

It is clear from Figure 5a that the size of the corrections needed for the move and rotate mode was significantly larger than the other two modes, with beam shifts of greater than 200 nm in both directions required frequently. For the small holder/rotate only mode the corrections were generally of the order of +/- 150 nm and during some parts of the process few corrections were needed at all. Despite the absence of sample movement, image shifts were still needed for the static mode, but these corrections were the smallest in magnitude of the three modes; where required almost all were between 50 and 90 nm and the four larger (< -100 nm) negative X shifts all followed reheating (conditioning) the ion beam tip and thus were not related to particular issues with sample stability (reheating effects were not observed in the other two data sets only because they were acquired at an earlier stage in the lifetime of the Ga+ ion source when the source was more stable). However, Figure 5b shows that the size of the individual corrections does not correlate with the overall drift of the sample during the course of each experiment. Both the rotate only and static modes show large cumulative shifts had to be applied on one axis in each case: in the rotate case this drifted on the Y axis (toward the detector) by over 2.5 µm before drifting back by about 1.5 µm. This drift will be discussed in Section 4.

The graphs of Figure 6 show the SEM image shift corrections corresponding to the FIB corrections of Figure 5. The individual SEM corrections shown in Figure 6a display a similar trend to those of the FIB in Figure 5a, with noise levels reducing from the move and rotate to rotate and thence to the static. It is however noticeable that the size of the shifts is generally greater for the electron images, and that for the latter two experiments the shifts are worst at the start of each run. In all three cases the cumulative shifts are large for one axis, but only for the static case is there an obvious correlation between the FIB and SEM corrections with the X direction shifts of similar magnitude but in opposite directions.

In the static case there is a large shift in the x_F direction and also similar magnitude in the x_S direction. Since the images are different views of the same object it is possible to correlate these movements. The FIB image contains only the x_3, z_3 plane and the SEM image has only the x_3, y_3 plane, but it is possible to compare x_3 data, the direction along the sample edge, from the two data sets. The resultant of the two SEM image shifts, x_s and y_S along the sample edge, x_3, can be calculated from the simple rotation of 54° between x_s and x_3. The resultant of this transformed SEM shift data is compared with that measured on the FIB image x_F, plotted as the red dotted line in Figure 5b. The near coincidence of the two shifts indicates that image shifts are due largely to sample drift, rather than individual beam movements.

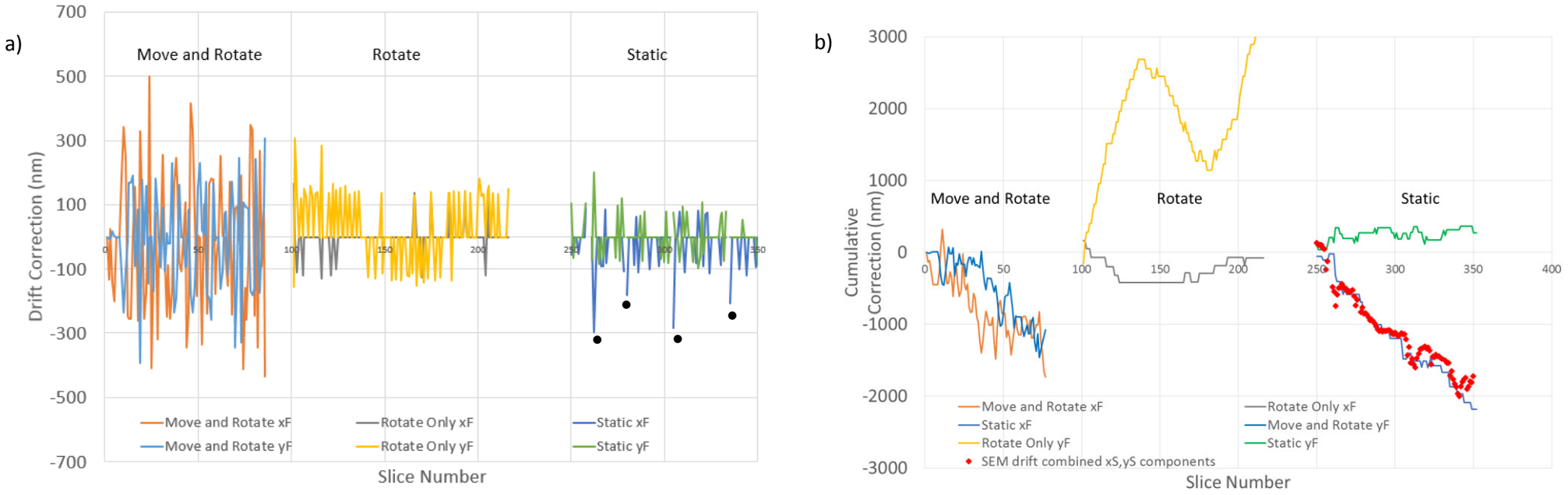

Figure 5. FIB beam displacement (drift correction)

a) change from slice to slice (• by four x_F points indicates realignment after ion beam reheat. b) cumulative change from start of milling

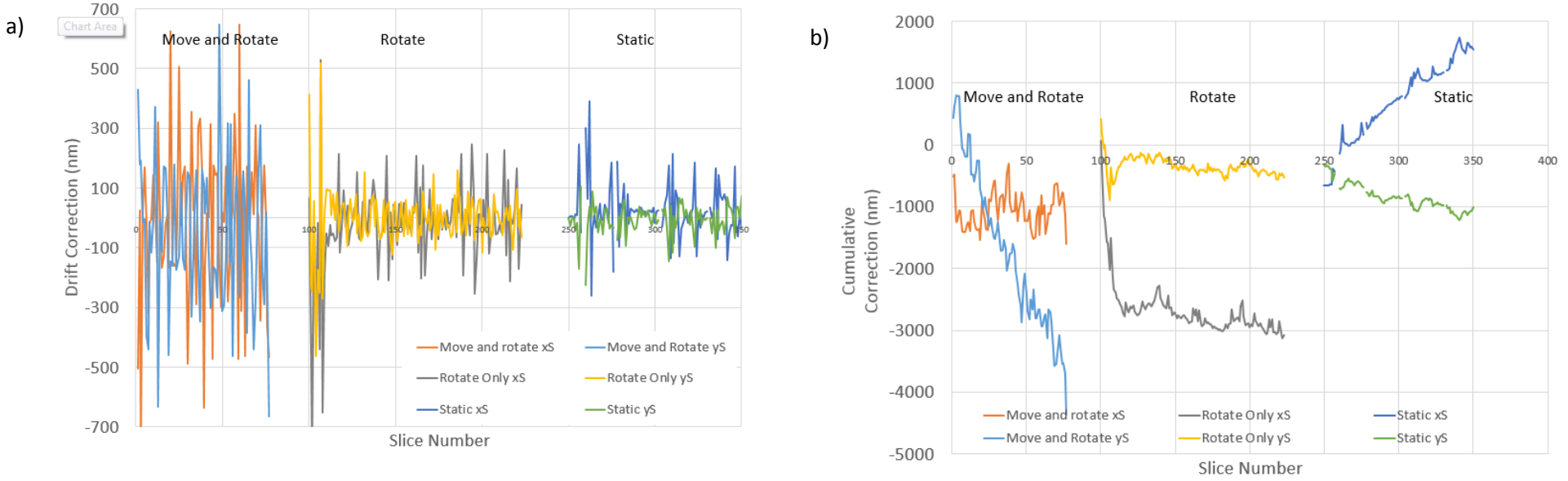

Figure 6. SEM beam displacement (drift correction) a) change from slice to slice and b) cumulative change from start of milling

3.2 3D Reconstruction of Datasets

For each of the three datasets the EBSD data was processed with Dream3D software [11], aligning the individual slices/EBSD maps with each other by applying a filter which minimises the total misorientation of each pixel in one map with its nearest neighbours in the next (starting with the final map and working back). Two views of the resulting 3D reconstructions are shown in Figure 7: the views of the y_3-z_3 plane in Figures 7d-f show the largest re-alignments required between slices, which were much greater parallel to the y_3-axis than the x_3-axis. The realignments in the x_3 and y_3 directions are quantified in Figure 8, with the shifts shown in number of pixels; the correspondence between the cumulative graphs and the Y-Z plane images is clearly seen. The shifts required for the Move and Rotate mode are more random than those for the other two modes; the Rotate only and the Static/Direct detector mode indicate systematic problems discussed later.

The improved level of indexing of the static detector over the conventional detector may also be noted from Figure 7, which, given the significant improvement in the pattern quality with albeit a relatively small increase in acquisition time (Figure 2), is perhaps not surprising.

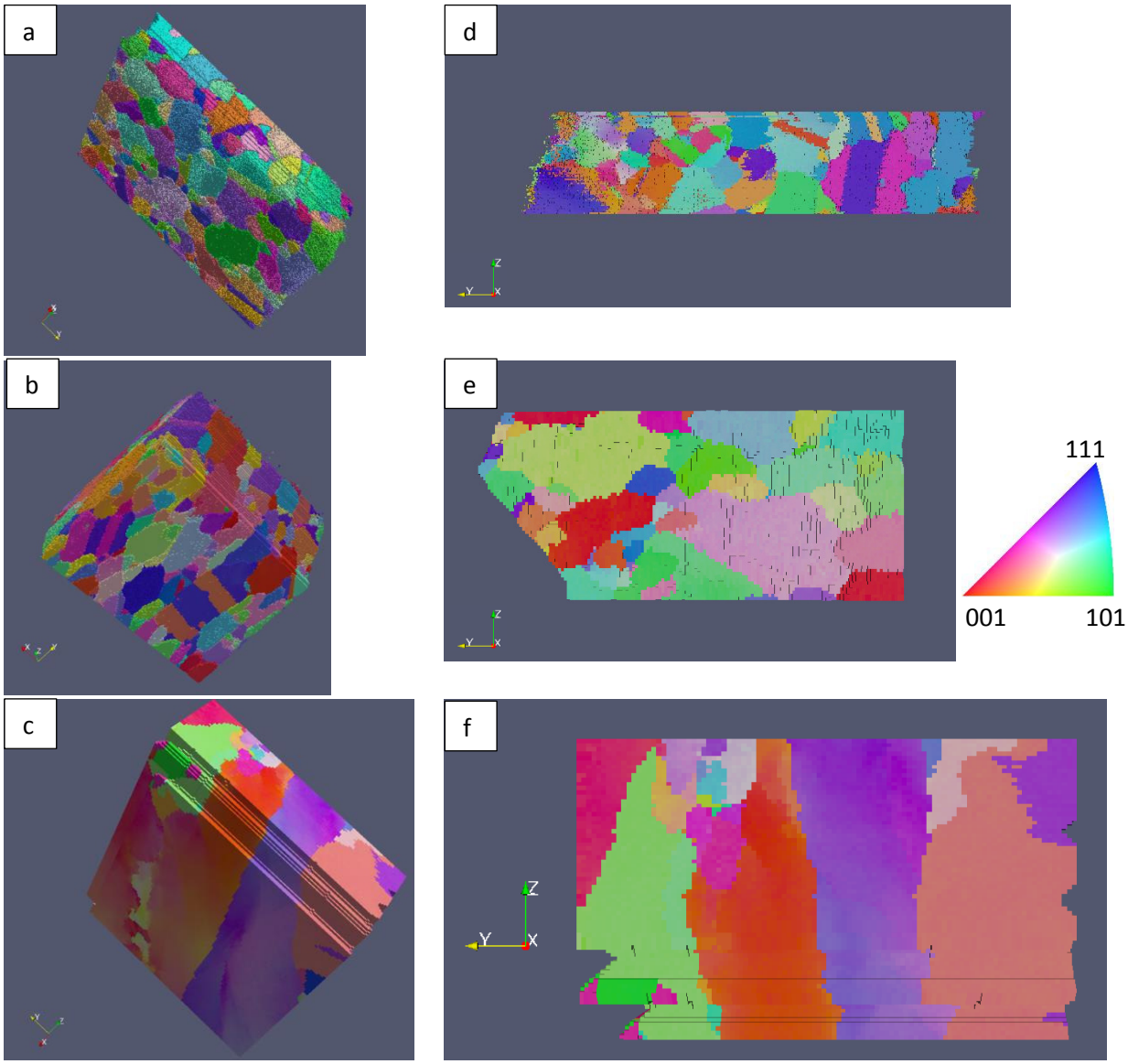

Figure 7. 3D reconstructions of Ni microstructures produced with Dream3D software:
a), d) Move and rotate mode, data dimensions ≈ 25 x 30 x 8 µm. b), e) Rotate only mode,

data dimensions ≈ 30 x 30 x 10 µm. c), f) Static mode, data dimensions ≈ 33 x 33 x 23 µm. Colours in grains show orientation based on the cubic inverse pole figure colour scheme shown.

4. Discussion

The data in Figures 5 and 6 show that the use of fiducial marks to reposition the beam relative to the sample at every change between FIB milling and SEM EBSD mapping is clearly essential for all three modes of operation. The reasons for these corrections vary between the modes, with some inherent to the mode used, but in the case of the static mode some corrections were specific to the microscope stability at the particular time of use: this section will discuss these reasons in more detail. The resulting data on post-acquisition alignment in Figures 7 and 8 show that the beam repositioning does achieve good alignment in the x_3 direction. However in the vertical direction, y_3, reconstruction of a 3D dataset for the two modes requiring sample movement generally does require further significant post-acquisition repositioning of the individual data slices, in agreement with the findings of Korte et al [12].

Note however that the post-acquisition repositioning does not take into account any variation in slice thickness in the z_3 direction that may have resulted from errors in the repositioning of the FIB beam (in the y_F direction of the FIB image in Figure 1). Figure 5 shows these corrections in y_F can be particularly significant for the two modes requiring sample movement, but given the alignment achieved in the final data for x_3 from the x_F corrections future work would be useful in future work to investigate if these y_F corrections improve the inherent variations in sequential slice milling which are known to cause variation of up to 20% even during stable static milling without EBSD mapping [13] or whether errors in the corrections add to the variation.

Considering the beam repositioning data in more detail, initially for the two modes involving sample movement, it is clear from Figures 5 and 6 that larger random corrections after each movement were needed by the Move and Rotate mode than the simple Rotate mode. The size of the corrections are still however smaller than the 1-3 µm that might be expected from likely stage repeatability [14]. The bigger correction in X (parallel to all three X directions, x_3, x_F, x_s as shown in Figure 2) for Move and Rotate might be expected because this mode moves +/- 50 mm compared with the +/-1 mm or less of the Rotate mode. However, by contrast, the magnitude of sample movement in the y_F direction for both modes is similar and despite this the y_F image corrections for the Move and Rotate mode were much larger than for the Rotate only and similar in magnitude to those of the x_F for this mode, suggesting the total distance moved was not the critical factor. Since the fiducial mark repositioning confidence levels were similar for both modes, the larger corrections of the Move and Rotate mode may indicate an additional effect of reduced stage repositioning accuracy caused by the larger mass of sample holder used in this mode, amplified by the fixed 17° tilt of the tall specimen holder.

The large random corrections needed for the Move and Rotate mode lead in general to the need for larger and generally random corrections to the final dataset alignment shown in Figure 8 (and possibly lead to reduced accuracy of alignment too). The final dataset alignment for the Rotate mode suggests the drift corrections in x_s were very accurate and that for this case the positioning accuracy discussed in [14], at least to the level of 0.1 µm, is achieved, although whether the "10s of nm" reported cannot be determined from this work.

,The clearly systematic problem in the y_3 direction for the rotate only dataset alignment (Figure 8b) results from a frequently encountered error in communication between the two sets of commercial software (the FIB and EBSD control software) and the failure to either exchange the correct beam

shift data or apply the correct beam shifts to compensate for movement of the front face of the sample with each milling step.

It should be noted that the y_3 corrections are probably required to compensate largely for the change in working distance between the FIB and EBSD positions, enabled by a movement of the microscope Z-stage by about 9 mm, in comparison with < 1 mm of the Y-stage for re-centring.

The beam correction and dataset realignment figures for the static mode do not immediately indicate a significant improvement in image stability that might be expected for this mode. However the sawtooth changes in the first 20 slices of the static data in Figure 8b are a consequence of the use of an incorrect value for compensation of the movement of the milled face relative to the fixed sample as each slice of material is removed. Once this parameter had been corrected mid-run the corrections needed were relatively small and infrequent.

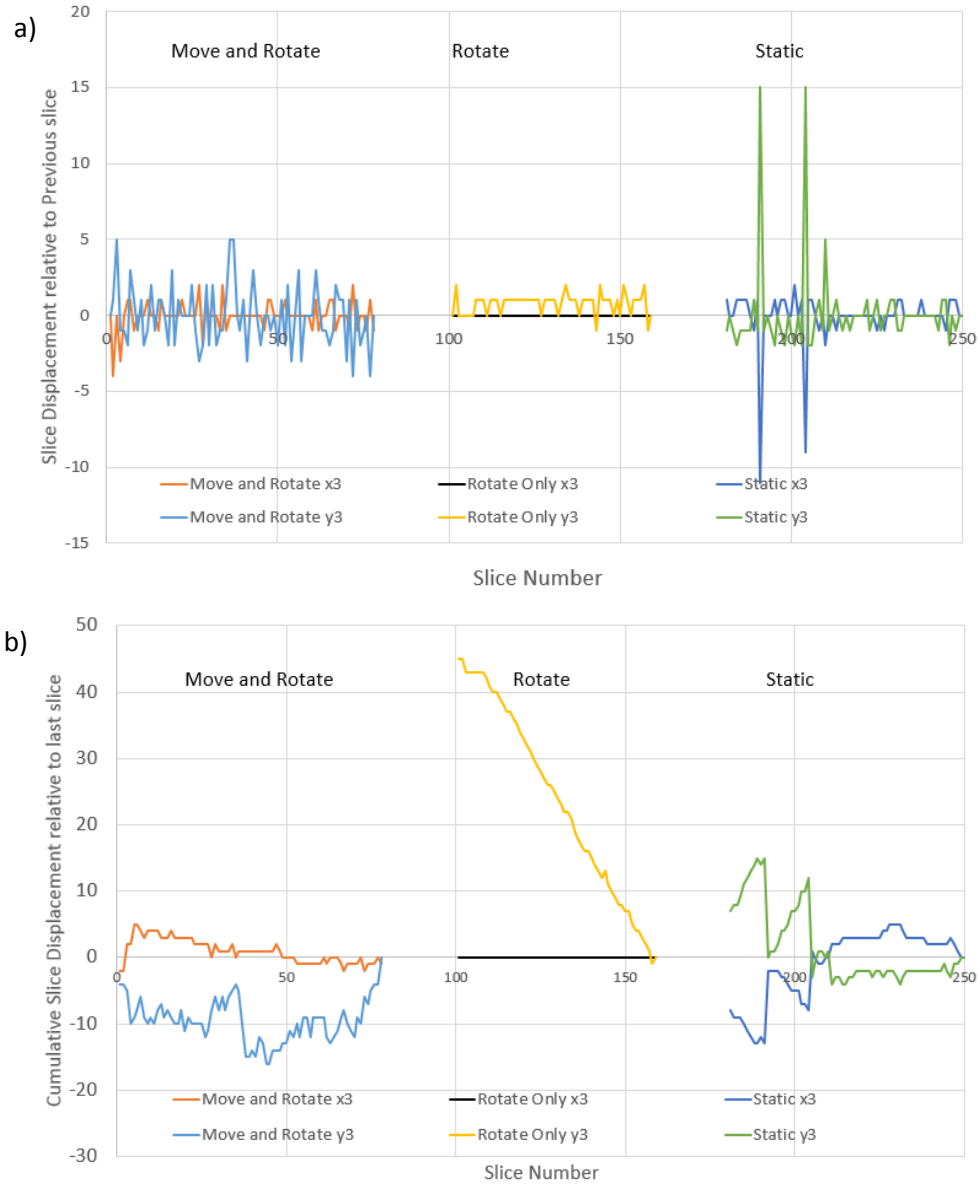

Figure 8. Map displacements (in units of pixels) calculated by Dream 3D to align with final slice a) change from slice to slice and b) cumulative change from final slice

However the magnitude of the total beam realignments needed for the static mode were still measureable after this correction and indicate that other factors require better control if the full benefits of this mode are to be realised. Firstly, the spikes noted for the FIB realignment (by a • in Figure 5a) resulted from reheating of the Ga ion tip; better tip conditioning to avoid the frequency of reheating seen here would reduce this problem, but it does indicate the need for beam realignment after any reheat. Secondly, there is still a systematic drift of the sample indicated by the diverging lines in Figures 5b and 6b. To explore a likely cause of this, a thermocouple was attached to the top of the sample holder base plate and the stage temperature monitored while a sample was imaged under the electron beam, without FIB milling) but with the direct detector on and recording continuously for 48 hours. Figure 9 plots the temperature and corresponding x and y positions of the sample, as measured from movement of the electron image.

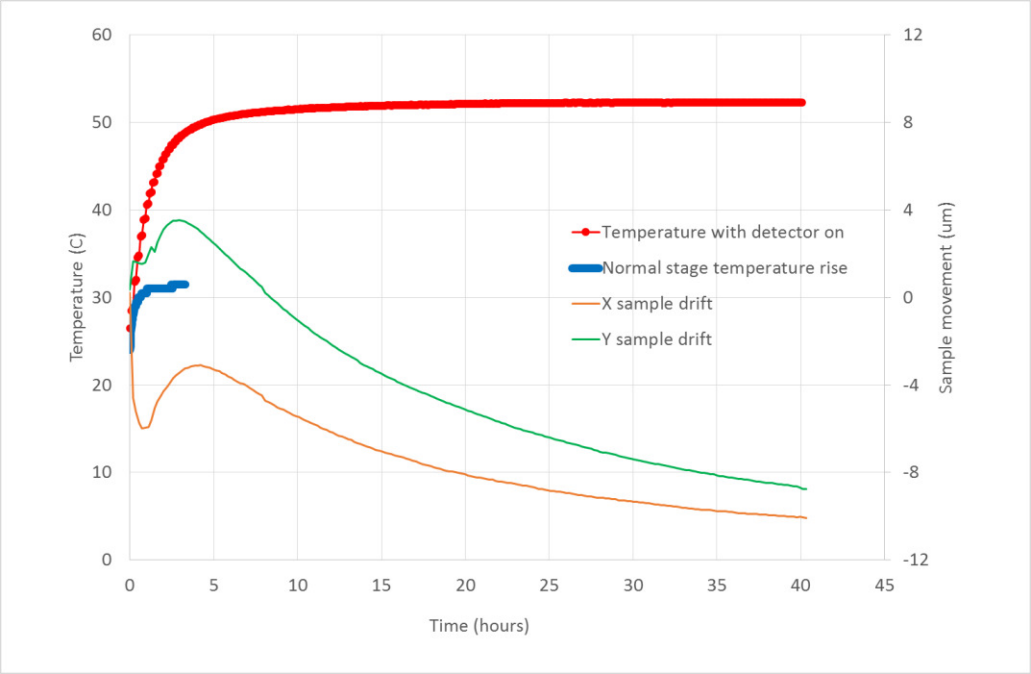

Figure 9. Stage drift measured for the static direct detector arrangement during continuous imaging without milling compared with temperature rise produced by the direct detector. For comparison the normal temperature rise produced over the course of 3 hours by the standard stage motors is also plotted.

It can be seen that the heat generated by the direct electron detector and its electronics is sufficient to double the stage temperature to over 52°C. The power consumption of the direct detector is ≈1W when attached to the USB cable, and goes up to ≈2.3W when the detector software is acquiring data. There is also an additional heat load of ≈0.7W from the 4 position sensors attached to the Smaract stages which contributes ≈5 °C to the overall temperature rise. The thermal load causes expansion of the detector assembly and the stage base which, combined with the different attachment positions of the detector and sample holder to the base, moves the sample relative to the detector and to the microscope axes. This leads to sample movement initially in a positive direction by up to 4 µm in both x and y directions, followed by drift of ≈ 7 µm and 13 µm in the negative direction for x and y respectively over 48 hours, a similar length of time to the 3D EBSD run. The stage base temperature stabilises after about 24 hours but the complex arrangement of Smaract stages holding the sample probably means the sample temperature takes much longer to equilibrate

and thus longer for the sample position to stabilise. On turning off the detector the stage temperature fell back to 34 °C, within a few degrees of that caused by the standard stage motors on the Zeiss microscope.

The drift noted in the x_F direction in Figure 5 is parallel with the direction in which the sample is suspended offset, above the baseplate and central SEM stage axis, by over 50 mm from where the Smaract stages are fixed to the baseplate. The baseplate is made of aluminium and for a length of 50mm would be expected to change in length by 1.15 µm per degree change in temperature. With the interfaces between the baseplate and Smaract stages/sample, a temperature difference between them is very likely so the overall magnitude of the sample movement measured is not surprising. During the actual static 3D dataset acquisition, at least 10 hours elapsed between the initial set up and acquisition starting, so the approximate drift of 2.5 µm noted in Figures 5 and 6 is consistent with the magnitude of the changes described here. The temperature induced stage drift is significantly higher than that measured during the 3D acquisition and shows a continuous smooth variation with a steadily reducing rate, whereas the variation measured by image correlation is noisy and the overall rate of drift does not reduce at all. Ion beam stability is clearly part of the cause as shown by the correlation of drift correction with tip conditioning; following a tip reheat the FIB drift corrections become noisier and surprisingly the SEM corrections follow a similar pattern. Instability of the ion beam positioning would be consistent with the previously observed [13] slice thickness variation of up to 20% from the set value for a static arrangement just producing SEM images but image drift was not measured in this earlier work. Without the thermal drift caused by the specific sample-detector arrangement used here the errors in slice alignment and thickness of the static mode should become just those inherent in the static slice and view technique summarised in [13] and [14].

One further experimental detail should be noted. After using detector in this geometry within 14 mm of the sample for over 48 hours, a thin discoloured band a few millimetres wide running across a portion of the detector surface was noted which was consistent with the trajectory of the ion beam. Further work has since used a shutter between sample and detector during milling which is retracted for EBSP acquisition.

5. Conclusions

The 3D EBSD datasets obtained together with positional data during their acquisition have demonstrated the capabilities and limitations of the different acquisition methods.

Results from the static sample arrangement with a direct electron EBSD detector were complicated by two issues specific to the precise construction and instrument condition, namely thermal drift and ion beam stability. Together, these necessitated image correlation and beam repositioning on alternating between EBSD and milling steps, even though most static “slice and view” arrangements without EBSD do not use this step.

However, if the thermal and beam stability effects are separated out, the static/direct electron detector arrangement did demonstrate better stability over the sample movement methods, with reduced post-acquisition alignment, especially in the Y_3 direction akin to conventional static slice and view methods. Furthermore, it was shown that the use of the direct electron detector is relatively straightforward to locate at the short working distance required by the FIB-SEM and at a small sample-detector separation with the potential for fast acquisition of good EBSD patterns

The results for the conventional methods involving sample rotation and varying levels of X-Y movement showed that minimising the sample holder size is likely to substantially reduce the corrections needed on alternating between milling and EBSD positions. The beam repositioning between stages was however shown to produce good alignment in the X_3 direction but as expected significant post acquisition Y_3 realignment is needed because no corrections are made for the change in sample working distance at each stage.

The minimal post-acquisition alignment needed in the X_3 direction for all the methods used following the beam repositioning during acquisition suggests that image correlation during conventional static slice and view will improve the repeatability of the slice thickness in the Z_3 direction, whichever method is used.

Acknowledgements

The work was funded by the National Measurement System of the UK Government Department for Business, Energy and Industrial Strategy

References

1. Direct Detection of Electron Backscatter Diffraction Patterns, A.J.Wilkinson, Grigore Moldovan, T.B.Britton, A.Bewick, R.Clough and A.I.Kirkland, PRL 111, 065506 (2013)
2. Digital direct electron imaging of energy-filtered electron backscatter diffraction patterns, S. Vespucci, A.Winkelmann, G.Naresh-Kumar, K.P.Mingard, D.Maneuski, P.R.Edwards, A.P.Day,V.O'Shea and C. Trager-Cowan Phys. Rev. B 92, 205301 (2015)
3. Present state of EBSD, R. A. Schwarzer, D. P. Field, B. L. Adams, M. Kumar and A. J. Schwartz, in *Electron Backscatter Diffraction in Materials Science*, edited by A. J. Schwartz, M. Kumar, B. L. Adams, and D. P. Field (Springer, New York, 2009), Vol. 2, Chap. 1, p. 1.
4. X. Llopart, R. Ballabriga, M. Campbell, L. Tlustos, and W.Wong, Nucl. Instrum. Methods Phys. Res., Sect. A 581, 485 (2007).
5. 10 years of the Medipix2 Collaboration M.Campbell, Nuclear Inst and Methods in Phys. Res. A 633 (2011) S1–S10
6. Advancing FIB assisted 3D EBSD using a static sample setup, J.Guyon, N.Gey, D.Goran, S.Chalal, F.Pérez-Willard, Ultramicroscopy 161 (2016) 161–167
7. 3D Orientation Microscopy, S .Zaefferer and S.I. Wright in *Electron Backscatter Diffraction in Materials Science*, edited byA. J. Schwartz, M. Kumar, B. L. Adams, and D. P. Field (Springer, New York, 2009), Vol. 2, Chap. 8, p. 109.
8. 3D reconstruction and characterisation of polycrystalline microstructures using a FIB–SEM system. Groeber, M. A., Haley, B., Uchich, M. D., Dimiduk, D. M. & Ghosh, S Mater. Charact. 57, 259–273.(2006)
9. http://www.advacam.com/en/products/modupix accessed Feb 2017
10. MAXIPIX, a fast readout photon-counting X-ray area detector for synchrotron applications, C.Ponchut J-M Rigal, Clement, S.Petitdemange, 2011 J. Instr. 6 C01069 DOI: 10.1088/1748-0221/6/01/C01069
11. DREAM.3D: A Digital Representation Environment for the Analysis of Microstructure in 3D, M.A.Groeber, M.A.Jackson, Integrating Mater. Manufacturing Innovation 3,5 (2014) http://dream3d.bluequartz.net
12. Three-dimensional electron backscattered diffraction analysis of deformation in MgO micropillars, S. Korte, M. Ritter, C. Jiao, P.A. Midgley and W.J. Clegg, Acta Mater. 59 (2011) 7241–7254
13. Investigation of slice thickness and shape milled by a focused ion beam for three-dimensional reconstruction of microstructures H.G. Jones, K.P.Mingard, D.C.Cox Ultramicroscopy 139,(2014),20–28
14. Metrological Challenges for Reconstruction of 3D Microstructures by Focused Ion Beam Tomography Methods, K.P.Mingard, H.G.Jones and M.G.Gee, J.Microsc. 253, 93–108, 2014